This article was downloaded by: [University of California, San Diego]
On: 28 September 2012, At: 22:47
Publisher: Taylor & Francis
Informa Ltd Registered in England and Wales Registered Number: 1072954 Registered office: Mortimer House, 37-41 Mortimer Street, London W1T 3JH, UK

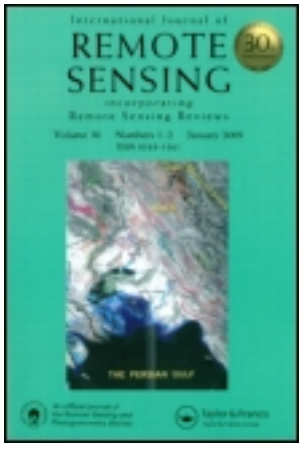

International Journal of Remote Sensing

Publication details, including instructions for authors and subscription information:
http://www.tandfonline.com/loi/tres20

Texture information-based hybrid methodology for the segmentation of SAR images

Pankaj K. Singh [a] , Nitesh Sinha [a] , Karan Sikka [a] & Amit K. Mishra [a]

[a] Department of Electronics and Communication Engineering, Indian Institute of Technology Guwahati, India

Version of record first published: 17 Aug 2011.

To cite this article: Pankaj K. Singh, Nitesh Sinha, Karan Sikka & Amit K. Mishra (2011): Texture information-based hybrid methodology for the segmentation of SAR images, International Journal of Remote Sensing, 32:15, 4155-4173

To link to this article: http://dx.doi.org/10.1080/01431161.2010.484821

PLEASE SCROLL DOWN FOR ARTICLE

Full terms and conditions of use: http://www.tandfonline.com/page/terms-and-conditions

This article may be used for research, teaching, and private study purposes. Any substantial or systematic reproduction, redistribution, reselling, loan, sub-licensing, systematic supply, or distribution in any form to anyone is expressly forbidden.

The publisher does not give any warranty express or implied or make any representation that the contents will be complete or accurate or up to date. The accuracy of any instructions, formulae, and drug doses should be independently verified with primary sources. The publisher shall not be liable for any loss, actions, claims, proceedings, demand, or costs or damages whatsoever or howsoever caused arising directly or indirectly in connection with or arising out of the use of this material.

International Journal of Remote Sensing
Vol. 32, No. 15, 10 August 2011, 4155–4173

Taylor & Francis
Taylor & Francis Group

Texture information-based hybrid methodology for the segmentation of SAR images

PANKAJ K. SINGH, NITESH SINHA, KARAN SIKKA and AMIT K. MISHRA*

Department of Electronics and Communication Engineering, Indian Institute of Technology Guwahati, India

(*Received 12 February 2009; in final form 19 August 2009*)

Image segmentation is one of the crucial tasks in the postprocessing of synthetic aperture radar (SAR) images. However, SAR images are textural in nature, marked by the textural patterns of widely disparate mean intensity values. This renders conventional multi-resolution techniques inefficient for the segmentation of these images. This article proposes a novel technique of combining both intensity and textural information for effective region classification. To achieve this, two new approaches, called Neighbourhood-based Membership Ambiguity Correction (NMAC) and Dynamic Sliding Window Size Estimation (DSWSE), have been proposed. The results obtained from the two schemes are combined, segregating the image into well-defined regions of distinct textures as well as intensities. Promising results have been obtained over the SAR images of Nordlinger Ries in the Swabian Jura and flood regions near the river Kosi in Bihar, India.

Downloaded by [University of California, San Diego] at 22:47 28 September 2012

1. Introduction

Synthetic aperture radar (SAR)-based imaging is an all-weather and day–night sensing system. Hence, SAR images are very crucial input for Earth mapping during routine assessments and also during disaster management programmes.

The current work deals with effective segmentation of SAR images. The images acquired by the SAR system often contain intricate textural patterns, including cases where similar textural patterns are observed for markedly different mean intensity values.

Early statistical methods for SAR image segmentation include methods based on the co-occurrence matrix (Lam 1996, Zwiggelaar 2004, Wu *et al.* 2008). The semi-automatic algorithm proposed by Bernad *et al.* (2007) uses the variation coefficient and co-occurrence inertia matrix for image classification into homogeneous regions. This is followed by 'Forest/Field' discrimination using costs based on certain potential functions. However, the article focuses on discerning Land/Forest areas only. Hence, it tends to lose generality and cannot be applied to other textural patterns. Further, since no justification has been provided for the usage of the inertia measure out of

*Corresponding author. Email: akmishra@ieee.org. Now at: Radar Remote Sensing Department, Department of Electrical Engineering, University of Cape Town, South Africa.

International Journal of Remote Sensing
ISSN 0143-1161 print/ISSN 1366-5901 online © 2011 Taylor & Francis
http://www.tandf.co.uk/journals
DOI: 10.1080/01431161.2010.484821

the 14 statistical features proposed by Haralick, the possibility of better results with other measures cannot be ruled out. Other methods include Gaussian Markov random fields, etc. (Haralick *et al.* 1973, Derin and Elliott 1987, Cohen *et al.* 1991, Manjunath and Chellappa 1991). But all these methods work satisfactorily only with a certain specific class of images. Also, their scopes are limited to spatial interactions over relatively small neighbourhoods, and hence, are suited only for microtexture (Unser, 1995). Of late, multi-resolution techniques like the Gabor filter (Haley and Manjunath 1995, Saito *et al.* 1996, Arivazhagan *et al.* 2006) have also been used for SAR image segmentation. However, Gabor filtering suffers from the drawback of non-orthogonality of the results. As a corollary of this, there is significant correlation between different textures (Arivazhagan and Ganesan 2003). They also require precise setting of different parameters (Chang and Kuo, 1993). The wavelet transform method (Mallat 1989, Unser 1995, Charalampidis and Kasparis 2002) belongs to the class of multi-resolution image filtering techniques which has been observed to be free from the drawbacks mentioned above. Several statistical tools (Laine and Fan 1993) applied in the wavelet sub-bands can be used for effective region classification of images at different scales.

The techniques described above work only for cases where the image is purely textural, that is, no information is contained in the intensity levels. However, if applied over images containing both intensity and texture variation, these tend to produce noisy results along with inaccurate region boundaries (Dubuisson-Jolly and Gupta 2000). For the above mentioned algorithms, the feature extraction or image pixel classification is based on the gradation of the intensity values and not on the values themselves. Dubuisson-Jolly and Gupta (2000) proposed a probabilistic model to deal with this issue. It employs maximum likelihood to cluster the data which is fitted over a Gaussian curve. However, the assumption of a particular class of distribution may not always fit the data accurately. Also, it uses a training data set for region classification. This makes the algorithm unsuitable for dealing with new modalities of texture types.

In this article, we present an innovative approach to segment SAR images, taking into account both intensity and textural variations. The approach uses a two-dimensional wavelet transform to segment the textural content of the image. It commences with the estimation of the coefficient matrix for four different resolution levels of the image. This is followed by a self-proposed method of Dynamic Sliding Window Size Estimation (DSWSE) based on image intensity variability. The window is slid over each of the corresponding coefficient matrices to obtain four variance matrices. The Modified Fuzzy *c*-Means (MFCM) approach is employed to cluster these matrices, providing us with the texture-based classified result. The original image is then segmented based on intensity using MFCM followed by a novel approach of Neighbourhood-based Membership Ambiguity Correction (NMAC). It removes most of the pixel level noise and also smooths the boundaries between abutted regions. Segmentation results from the above two methods are fused together to obtain the final output. Figure 1 shows the diagrammatic representation of the whole algorithm.

2. Wavelet transform

Wavelet analysis (Mallat 1989) is a contemporary approach developed for multi-resolution representation of signals. It has the advantage of being localized in the time

Downloaded by [University of California, San Diego] at 22:47 28 September 2012

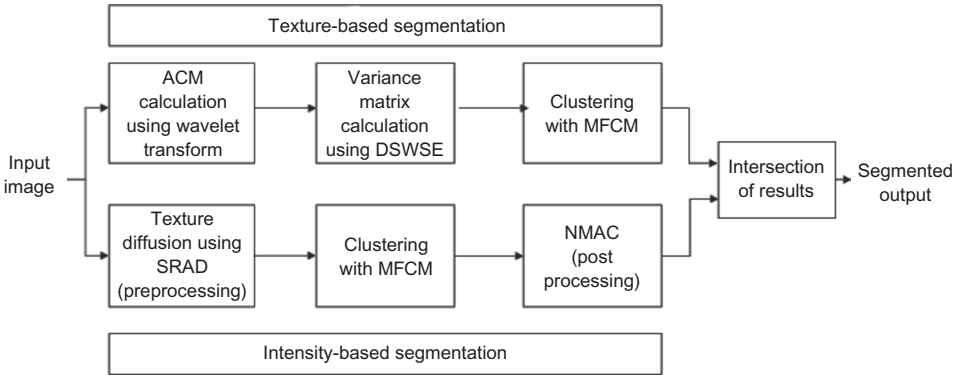

Figure 1. Diagrammatic representation of the whole algorithm.

as well as the frequency domain over its counterparts, like the Fourier transform or discrete cosine transform which are localized in the frequency domain only. A signal is decomposed into both translated and dilated versions of a single function called the mother wavelet Ψ given as

$$\Psi_{a,b}(x) = \frac{1}{\sqrt{a}}\Psi\left(\frac{x-b}{a}\right) \tag{1}$$

where a is the scaling parameter, b indicates the translation of the mother wavelet and x is the independent variable in the continuous wavelet transform.

Replicating the same in the discrete domain, the discrete wavelet transform can be calculated using a filter bank consisting of a set of quadrature mirror filters, $\tilde{\boldsymbol{G}}$ and $\tilde{\boldsymbol{H}}$, at each level. Here, $\tilde{\boldsymbol{G}}$ and $\tilde{\boldsymbol{H}}$ are the frequency responses of a low-pass and a high-pass filter, $\tilde{g}(-n)$ and $\tilde{h}(-n)$ being their impulse responses, respectively.

Passing the signal through this filter bank results in a set of two outputs at each level given as

$$\boldsymbol{A}_{2^j}^d = \sum_{k=-\infty}^{\infty} f(k)\,\tilde{g}(2n-k) \tag{2}$$

$$\boldsymbol{D}_{2^j}^d = \sum_{k=-\infty}^{\infty} f(k)\,\tilde{h}(2n-k) \tag{3}$$

where $\boldsymbol{A}_{2^j}^d$ is the discrete approximation signal and $\boldsymbol{D}_{2^j}^d$ is the discrete detail signal of a function $f(x)$ at resolution 2^j (Mallat 1989).

We proceed by taking the wavelet transform of the complete image using a Haar wavelet as the mother wavelet. This concept can easily be extrapolated to two-dimensional signals, as shown in figure 2, to obtain the following four components:

(i) low-frequency coefficient, $\mathbf{A}_{2^j}^d$;
(ii) vertical high-frequency coefficient, $\mathbf{D}_{2^j}^1$;
(iii) horizontal high-frequency coefficient, $\mathbf{D}_{2^j}^2$; and
(iv) high-frequency coefficient in both the horizontal and vertical directions, $\mathbf{D}_{2^j}^3$.

Downloaded by [University of California, San Diego] at 22:47 28 September 2012

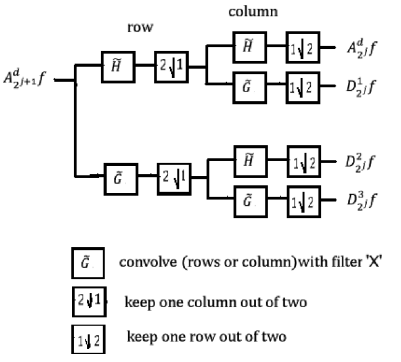

Figure 2. Frequency-based image segregation into sub-bands at a single level.

3. Modified FCM

Conventional Fuzzy *c*-Means (FCM) clustering algorithms (Lin *et al.* 1996) suffer from the drawback of considering pixels as independent units. This makes them more sensitive to noise. There is much previous work in the open literature aimed at finding a solution to this problem by using localized spatial information like the neighbourhood effect (Chumsamrong *et al.* 2000, Ahmed *et al.* 2002). As per these algorithms, a pixel's membership grade is also affected by those of its neighbouring pixels. The neighbourhood consideration mitigates the effect of noise on a pixel. One such algorithm is proposed by Yong *et al.* (2004), where the membership grade, $\mu_{i,j}$, of each pixel and the cluster centre are updated using a parameter $p_{i,j}$, called the weight, which represents the probability of the i^{th} pixel belonging to the j^{th} cluster and is determined using the neighbourhood model. In each iteration of conventional FCM, $\mu_{i,j}$ is updated to $\mu^*_{i,j}$ according to the following equation:

$$\mu^*_{i,j} = \mu_{i,j} p_{i,j} \tag{4}$$

where,

$$\mu_{i,j} = \frac{\left(\frac{1}{(d_{i,j})^2}\right)^{1/(m-1)}}{\sum_{l=1}^{c}\left(\frac{1}{(d_{i,l})^2}\right)^{1/(m-1)}}\,. \tag{5}$$

Here, $d_{i,j}$ is the distance between the i^{th} pixel and the j^{th} cluster centre, m is a fuzzification parameter, and c is the number of cluster centres. The cluster centre, w_j, in the next iteration is updated accordingly using $\mu^*_{i,j}$ in place of $\mu_{i,j}$ in equation (6):

$$w_j = \frac{\sum_{i=1}^{M} \mu^m_{i,j} x_i}{\sum_{i=1}^{M} \mu^m_{i,j}}. \tag{6}$$

Here, x_i is the intensity value of the i^{th} pixel and M is the total number of pixels in the image. The method proposed for determining the weight $p_{i,j}$ is inspired from the

Downloaded by [University of California, San Diego] at 22:47 28 September 2012

k-nearest neighbour (k-NN) algorithm and is computed according to the following formula:

$$p_{i,j} = \frac{\sum_{l \in N_j} \frac{1}{1+\alpha\left(d_{l,j}\right)^2}}{\sum_{l \in N_i} \frac{1}{1+\alpha\left(d_{l,j}\right)^2}}. \tag{7}$$

Here, α is a positive constant, N_i is a set of k nearest pixels of the i^{th} pixel and N_j is the subset of N_i consisting of pixels belonging to the j^{th} cluster.

4. Proposed algorithm

Real life SAR images are accompanied by a variety of distinct aspects, all of which should be dealt with subtlety during analysis. Certain classes of images consist of both intensity and textural variations (Dubuisson-Jolly and Gupta 2000, Sun *et al.* 2008). Segmentation of these images based on intensity or texture alone produces erroneous results.

For correct classification, any two pixels in the image should be graded into the same region if and only if they correspond to the same texture and the same intensity region simultaneously; or else, they should be classified into distinct regions. To address this requirement, intensity- and texture-based classification has been proposed (Dubuisson-Jolly and Gupta 2000, Sun *et al.* 2008). Working on similar lines, this article presents a novel algorithm for segmentation of the above-mentioned class of images. Texture-based segmentation has been executed with wavelet analysis at its core, while intensity-based segmentation is carried out with MFCM. The following two subsections describe these two algorithms.

4.1 *Texture-based segmentation*

4.1.1 Evaluation of coefficient matrices. We proceed by taking the wavelet transform of the complete image using a Haar wavelet as the mother wavelet.

This gives us the low-frequency coefficient, $\mathbf{A}^d_{2^j}$, the vertical high-frequency coefficient, $\mathbf{D}^1_{2^j}$, the horizontal high-frequency coefficient, $\mathbf{D}^2_{2^j}$ and the high-frequency coefficient in both the horizontal and vertical directions, $\mathbf{D}^3_{2^j}$ at the first level as described in section 2.

In conventional approaches, the four coefficient matrices so obtained are downsampled as shown in figure 2. However, the representation does not conserve an essential property, that is, invariance by translation. This article offers a solution by the use of an over-complete wavelet decomposition called the Discrete Wavelet Frame (DWF) (Unser 1995). This results in better retention of textural characteristics and more detailed region boundaries.

4.1.2 Dynamic Sliding Window Size Estimation (DSWSE). The coefficient matrices provide us with the frequency characteristics along with spatial localization, that is, they not only contain the information about the frequency distribution but also the spatial location of different frequencies. Evaluation of these matrices is followed by a channel variance calculation algorithm using a sliding window over each of the matrices. This gives us a localized trait around each pixel in the form of a variance matrix for each of the four resolution levels.

Downloaded by [University of California, San Diego] at 22:47 28 September 2012

A texel is the fundamental element of a texture, whose repetition over a plane yields a texture pattern. Greater variance within the window as defined above corresponds to a greater range of frequencies present in it, which in turn is a direct indicator of the smaller size of a texel. However, the size of the window plays a crucial role in extracting the textural aspects. In an image, the texel size contains the information regarding the approximate periodicity of the textural pattern. Images having comparatively smaller texel size will be accompanied by a higher number of sub-texel regions corresponding to a particular gradient. This is because a larger number of data points will be covered in forming the pattern. These types of images will require smaller windows to cover a texel. So, the window to be chosen should be small enough so that it may not diffuse the boundaries. At the same time, it should be large enough so as to contain a texel. These two conditions necessitate capping the size. This advocates the need for an image dependent window size.

A new algorithm based on the gradient of each of the coefficient matrices is proposed here. In order to calculate the variance, a window is taken such that its size is smaller than the texel sizes of most textures and hence ensures the retrieval of intra-texel features. Experimental observations advocate a sliding window of size ranging from 3×3 to 7×7 to ensure this. We have used a window of 5×5 pixels. The variance matrix is calculated using the following equation:

$$\sigma_{k,l} = \sum_{i=k-2}^{k+2} \sum_{j=l-2}^{l+2} (x_{i,j} - \mu_{k,l})^2 \tag{8}$$

where,

$$\mu_{k,l} = \frac{1}{25} \sum_{i=k-2}^{k+2} \sum_{j=l-2}^{l+2} x_{i,j}. \tag{9}$$

Here, $x_{i,j}$ represents the data point at position (i, j) in the coefficient matrix, and $\mu_{k,l}$ and $\sigma_{k,l}$ are the mean and variance, respectively, of the window centred at position (k, l) in the coefficient matrix.

The resultant matrix characterizes the actual textural information at the corresponding resolution level. The gradient of this matrix is taken, which supplies us with the rate of variability of the textural pattern over the whole image. The following equation is used for estimating the gradient, ϑ, at position (k, l) in the matrix obtained above:

$$\vartheta_{k,l} = [(\sigma_{k+1,l} - \sigma_{k,l})^2 + (\sigma_{k,l+1} - \sigma_{k,l})^2]^{1/2}. \tag{10}$$

A histogram of the gradient matrix shows that the majority of the information regarding the nature of the textural image with respect to the periodicity, the rate of intensity variation, etc., is mostly contained at the beginning of the whole gradient range. Further, the following information can also be interpreted from the histogram in order to explain the subtleties in its profile:

(i) A large percentage of the whole area of the histogram in the starting region corresponds to a dominantly slowly varying texture. For such images, a larger window is required for effective region classification.

Downloaded by [University of California, San Diego] at 22:47 28 September 2012

(ii) A smaller percentage of area signifies a primarily fast varying textural pattern and is expected to give better results with a comparatively smaller window.

Thus, it can be observed that the size of the window has a relationship to the distribution of the gradient values on the histogram. Thus in order to obtain the size automatically, the following methodology has been employed. The gradient range of each of the four variance matrices is plotted in the form of a histogram divided into 50 bins in order to achieve a significant level of resolution. In this case, the first three bins have been found to constitute the major portion of the gradient distribution. Hence, the information contained in these three bins has been used to determine the size of the window. To make the process automated, a third-degree polynomial was obtained with the independent variable as the percentage of data points falling in the initial three bins of the gradient histogram and the dependent variable as the window size. It has been experimentally verified that fitting over a second-order polynomial does not provide enough flexibility to the window size and hence leads to poor estimates. Experimentation with higher degree polynomials results in the coefficients of fourth and higher order components becoming nearly zero. Thus, a third-degree polynomial is chosen as it has the advantage of superior estimates without much computational load.

The polynomial so obtained has been tested with other synthetic images and has been found to provide encouraging results (section 5).

4.1.3 Calculation of the variance matrix. Once the window size is determined, the next step is to calculate the variance over a sliding window run over the corresponding coefficient matrix:

$$v_{k,l} = \sum_{i=k-w/2}^{k+w/2} \sum_{j=l-w/2}^{l+w/2} (x_{i,j} - \mu_{k.l})^2 \tag{11}$$

where,

$$\mu_{k,l} = \frac{1}{w^2} \sum_{i=k-w/2}^{k+w/2} \sum_{j=l-w/2}^{l+w/2} x_{i,j} \tag{12}$$

where w is the window size determined using DSWSE. The window size is always chosen to be even.

This furnishes us with the variance matrix

$$\mathbf{V} = \{v_{k,l}\} \tag{13}$$

which contains all the textural information of the corresponding component of the image. The data contained in the four $\mathbf{V}$ matrices is clustered using an extension of the MFCM approach (as described in section 3) in four dimensions. In this case, the Euclidean distance is taken between any two data points given by

$$d_{i,j} = \sqrt{\sum_{n=1}^{4} (v_{i,j}^n - w_j^n)^2} \tag{14}$$

Downloaded by [University of California, San Diego] at 22:47 28 September 2012

where $v_{i,j}^n$ is the value at the $(i,j)^{\text{th}}$ position of the n^{th} variance matrix. Similarly, w_j^n is the j^{th} cluster centre of the n^{th} variance matrix. Since the number of textural regions is visually perceivable, the number of clusters is fed manually into the MFCM algorithm.

4.2 *Intensity-based segmentation*

4.2.1 Diffusion of image (texture suppression). Ordinary intensity-based segmentation techniques such as those described by Pratt (2001) cannot be used directly on textural images. The reason is that texture in an image is fundamentally perceived by the pattern of intensity variations. So applying the intensity algorithms directly will assign multiple classes within a single textural region. In order to avoid this, we use the Speckle Reducing Anisotropic Diffusion (SRAD) (Yu and Acton 2002) technique in a novel way. The filter threshold is set so as to diffuse the texture details from an image. However, since the filter is adaptive, it protects the region boundaries from getting diffused. Another advantage of its adaptability is that the smooth portions of the images are not affected by the filter. This provides us with a smooth image which is segmented using MFCM.

4.2.2 Neighbourhood-based Membership Ambiguity Correction (NMAC). After the application of MFCM to the unbiased and contrast-enhanced image, we obtain an interim segmented image. In the process of clustering according to the final membership function **U** found by MFCM, a number of pixels are encountered where the difference in their membership grades for two clusters is low. Regions in the proximity of the boundaries have been found to be attributed with this characteristic. Pixels in such regions are marked with fairly close intensity levels and constitute a set of 'ambiguous pixels'. These pixels form smudged boundaries between different textural classes. In normal FCM or MFCM, such pixels are classified into that cluster for which their membership grade is maximum. However, this may lead to misclassification as the extent of associativity to a particular class is uncertain. This poses a problem in accurately determining the area of any specific region in SAR images. To find a solution for this issue, we present a method based on the neighbourhood effect.

We define ambiguous pixels as those in which the difference between the maximum and any other value of its membership grade is less than 0.15. The segmentation result for figure 3(*a*) is shown in figure 3(*b*). In this, the ambiguous pixels are shown in white. Experimental observations for such cases show that the pixels constituting the periphery of these smudged boundaries are less ambiguous than the inner ones. Since the identification of ambiguities is dependent upon the spatially neighbouring pixels, the outer pixels should be corrected first followed by the inner ones. This is because the outer pixels have greater probability of having a larger number of correctly classified pixels as their neighbours as compared to the inner pixels. Taking a cue from this hypothesis, the set of ambiguous pixels, A, is divided into three subsets according to the extent of the ambiguity:

$$\begin{aligned} A_1 &= \{x_i | x_i \in A \ \&\ |\mu_{i1} - \mu_{i2}| < 0.05\}, \\ A_2 &= \{x_i | x_i \in A \ \&\ 0.05 \leq |\mu_{i1} - \mu_{i2}| < 0.1\}, \\ A_3 &= \{x_i | x_i \in A \ \&\ 0.1 \leq |\mu_{i1} - \mu_{i2}| < 0.15\} \end{aligned} \tag{15}$$

Downloaded by [University of California, San Diego] at 22:47 28 September 2012

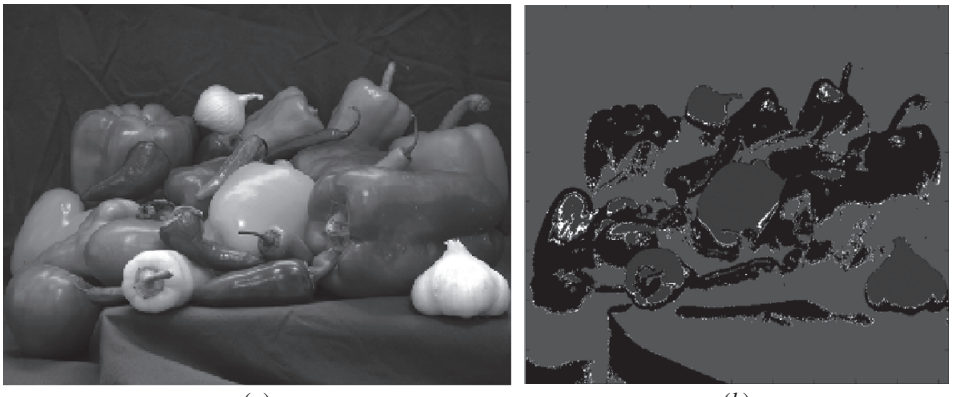

(*a*) (*b*)

Figure 3. (*a*) Still image, and (*b*) segmented result showing ambiguous pixels in white colour.

Downloaded by [University of California, San Diego] at 22:47 28 September 2012

such that

$$A = A_1 \cup A_2 \cup A_3 \tag{16}$$

where x_i represents the i^{th} pixel in the image and $\mu_{i,1}$ is $\max\{\mu_{i,j}\}$ and μ_{i2} is $\max\{\mu_{i,j} \backslash \mu_{i,1}\}$ $\forall j \in \{1, \ldots, c\}$ and c is the number of cluster centres.

We define C as the set of correctly classified pixels given by

$$C = \{x_i | x_i \notin A\}. \tag{17}$$

The sets A_3, A_2 and A_1 represent the increasing orders of ambiguity. It has been experimentally found out that the pixels constituting the outer portions of blurred boundaries are less ambiguous than the inner ones. Hence, in such cases, the outer pixels should be corrected first followed by the inner pixels. The reason behind this is that the pixels in the outer portions of the boundaries have a higher probability of having correctly classified pixels as their neighbours than the inner pixels.

We first consider N, the set of nearest neighbours of the i^{th} pixel, where $x_i \in A_3$. We define N_c as the set of neighbours of the i^{th} pixel which are distinctly classified, as given by

$$N_c = N \cap C. \tag{18}$$

Consider $\theta_{i,k}$ such that

$$\theta_{i,k} = \begin{cases} 1 & \text{if} \quad \mu_{i,k} = \mu_{i,1} \\ 0 & \text{otherwise.} \end{cases} \tag{19}$$

Now the i^{th} pixel belongs to the k^{th} cluster if

$$\sum_{x_i \in N_c} \theta_{i,k} = \max\left\{ \sum_{x_i \in N_c} \theta_{i,j} \right\} \qquad \forall j \in \{1, \ldots, c\}. \tag{20}$$

If the above equation becomes valid for some other cluster, l also, then the i^{th} pixel belongs to the k^{th} cluster if

$$\sum_{x_i \in N_c} \mu_{i,k} > \sum_{x_i \in N_c} \mu_{i,l}. \tag{21}$$

Otherwise it belongs to l.

The above procedure is repeated for all the points of A_3, after which we proceed to points of A_2 and then finally to those of A_1. The results obtained are observed to be of significantly improved quality.

4.3 *Combining results of texture- and intensity-based segmentation*

The final result of the segmentation process is produced by combining together the output results of the texture- and intensity-based segmentation.

In order to segregate the different regions, a primary visual inspection is done to identify the number of distinct textural regions. This is followed by the texture-based segmentation algorithm as defined in section 4.1. After this, a broad estimation of the number of intensity regions is made which is followed by intensity-based segmentation, elaborated in section 4.2. Since the user has a primary notion regarding the type and location of different regions, he/she will select two of the interim results, one from texture-based segmentation and the other from intensity-based segmentation encompassing a common region (rough land, smooth land or water) and will combine them together by taking a pixel by pixel intersection of each of the textural regions with all the intensity-based segmented regions. This approach is equivalent to the condition that a pixel is classified in a particular region if and only if it has both its intensity as well as its textural characteristics similar. This procedure is repeated for all the regions.

Alternatively, each of the interim results of texture-based segmentation is combined with all the results of intensity-based segmentation. Different regions can be retrieved from the results so produced by training the algorithm based on the mean intensity of various regions existing in the image. The training sets so obtained would be sensor and scene specific.

Other combinations of the interim results yield crass outputs. This has also been verified in the next section (figure 9).

5. Results and discussion

In this section, we evaluate the performance of the proposed algorithm. First of all, we present the utility of DSWSE by presenting a quantitative as well as a qualitative assessment of the results based on various parameters. This is followed by a depiction of the utility of calculating the coefficient matrices without downsampling. These two parts of the analysis are implemented over synthetic texture images. After this, a tabular presentation of the results with other synthetic images is given. Following this, the utility of NMAC is shown using a synthetic image to which noise was added. The testing is then relayed to qualitative evaluation of the results of this segmentation approach over SAR images made available by the ScanEx Research and Development Center. These data have been acquired using TerraSAR-X technology developed by DLR, German Aerospace Center (Buckreuss *et al.* 2003). The images are that of Nordlinger Ries in the Swabian Jura.

Downloaded by [University of California, San Diego] at 22:47 28 September 2012

In the first part, we present the efficacy of the textural-based segmentation algorithm built over DSWSE and un-downsampled coefficient matrices. For this, we have taken a synthetic image consisting of two different texture regions as shown in figure 4(*a*). Three different operations are done on this image:

(i) A fixed window size of 30×30 is chosen for calculating the variance matrix from the un-downsampled coefficient matrices. The segmentation result for this operation is shown in figure 4(*b*).
(ii) Window sizes are determined for the coefficient matrices obtained from the DSWSE method. The computed histogram for only the low-pass component is shown in figure 4(*c*). The calculated windows are used to obtain the corresponding variance matrices from downsampled coefficient matrices. The result is given in figure 4(*d*).
(iii) Window sizes are determined for the coefficient matrices obtained from the DSWSE method. In contrast to the above description, this window is used for calculating the variance matrix from the un-downsampled coefficient matrices. The corresponding result is shown in figure 4(*e*).

It can be easily observed that the result in the third case is markedly better than both the output obtained with the fixed window size and that obtained with the downsampled coefficient matrices.

Moving on to the quantitative analysis of the results, we first define the parameters used for the assessment. Performance analysis is based on two figures of merit: the sensitivity index (ρ) (Anbeek *et al.* 2005) and the similarity index (τ) (Zijdenbos *et al.* 1994). For calculating these figures of merit, we first find the True Positive (t_I), True Negative (t_{II}), False Positive (f_I) and False Negative (f_{II}) parameters for the results. Pixels classified in the correct region are referred to as true, else false. The pixels that are observed to be classified into a particular region are termed as positive while those that are not, are called negatives.

Given the above four parameters, the sensitivity, ρ, is given as

$$\rho = \frac{t_{\mathrm{I}}}{t_{\mathrm{I}} + f_{\mathrm{II}}} \tag{22}$$

and the similarity index, τ, is given by

$$\tau = \frac{2t_{\mathrm{I}}}{S + R} \tag{23}$$

where S refers to the observed segmentation while R refers to the correct results.

The calculated values of the above parameters for the results of the synthetic image in figure 4(*a*) are shown in table 1. The results with the estimated window show considerable improvement for both parameters. Table 2 shows the statistical results for three different synthetic images as shown in figure 5(*a*), (*b*) and (*c*). The results for the same are shown in figure 5(*d*), (*e*) and (*f*). Figure 6 shows how the NMAC technique removes the pixel level noise and also introduces smoothing of the boundary between the segmented regions.

Figure 7(*a*) shows a real SAR image of Nordlinger Ries in the Swabian Jura. The image consists of a wide variation in texture, from farmlands to inhabited areas. In addition to this, the smooth region (farmlands) of the image also shows local intensity

Downloaded by [University of California, San Diego] at 22:47 28 September 2012

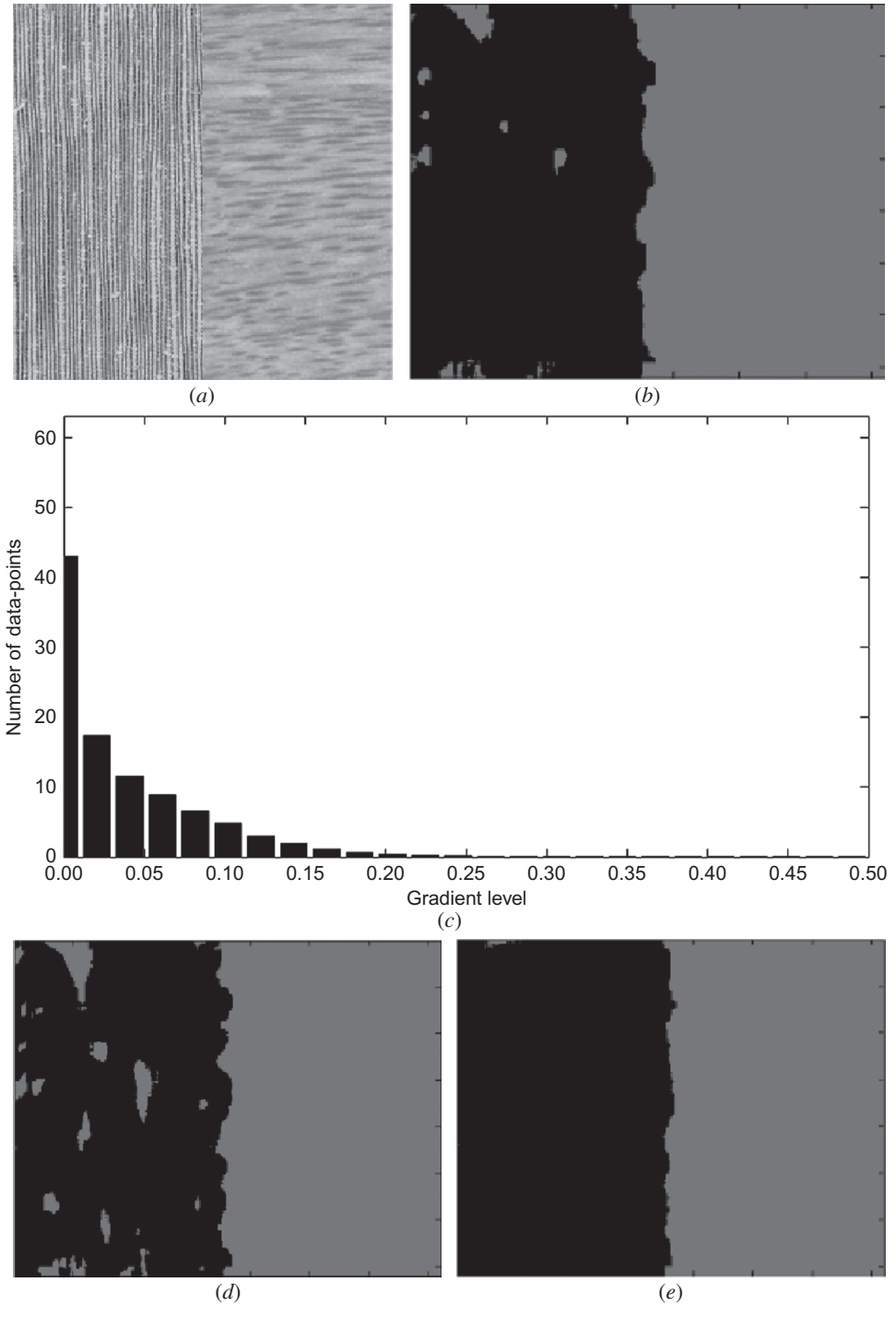

Figure 4. (*a*) Synthetic test image, (*b*) segmentation result with fixed window size 30 × 30 over un-downsampled coefficient matrices, (*c*) histogram of the gradient of variance of low-frequency coefficient matrix for first test image, (*d*) result of segmentation with evaluated window size over downsampled coefficient matrices and (*e*) segmentation result with evaluated windows size over un-downsampled coefficient matrices.

Downloaded by [University of California, San Diego] at 22:47 28 September 2012

Table 1. Comparison of the results of the segmentation of the test image obtained from the three operations explained above.

	Sensitivity (ρ)		Similarity index (τ)	
	Region 1	Region 2	Region 1	Region 2
Operation 1	0.9514	0.9958	0.9729	0.9742
Operation 2	0.9170	0.9954	0.9544	0.9578
Operation 3	0.9875	0.9973	0.9923	0.9925

Table 2. Statistical analysis of textural segmentation results for Image 1, Image 2 and Image 3.

	Sensitivity (ρ)		Similarity index (τ)	
	Region 1	Region 2	Region 1	Region 2
Image 1	0.9890	0.9691	0.9793	0.9789
Image 2	0.9936	0.9893	0.9908	0.9918
Image 3	0.9913	0.9967	0.9940	0.9940

Downloaded by [University of California, San Diego] at 22:47 28 September 2012

variations. Evidently, the image is fit to be classified primarily into four regions: the inhabited area and three distinct type of farmlands.

Figure 7(*b*) and (*c*) shows the result of texture-based segmentation as defined in section 4.1 with two clusters. Figure 7(*d–f*) shows the result of segmentation based upon intensity described in section 4.2. The final result so obtained after combining the above results using the procedure defined in section 4.3 is shown in figure 8(*b–e*). This example shows the effectiveness of the current algorithm over individual techniques of intensity and texture-based segmentation.

Figure 9 shows one of the outputs of the combination of non-corresponding interim results. A small number of pixels are covered under it, containing exiguous information.

The results depict the utility of using the approach of parallel segmentation based on intensity and texture.

The algorithm has also been tested upon airborne SAR images (Sharma *et al.* 2008) of flood inflicted areas near the Kosi River in Bihar, India. The images have been provided by the Indian Space Research Organization (ISRO) which has also appreciated the results. However, because of the airborne nature of the images, these are classified in nature and hence are not to be reproduced in this correspondence.

6. Conclusion

We have devised a new scheme to segment SAR images. A high level of accuracy has been achieved with synthetic test images. The outputs obtained over real SAR images, facilitated by ScanEx, have also been found to be particularly encouraging. We begin by evaluating the coefficient matrices for the image using wavelet analysis. This is followed by an innovative technique of window size estimation, DSWSE. Variance matrices are generated by sliding the windows over the corresponding coefficient matrices and then taking the average. These variance matrices are segmented

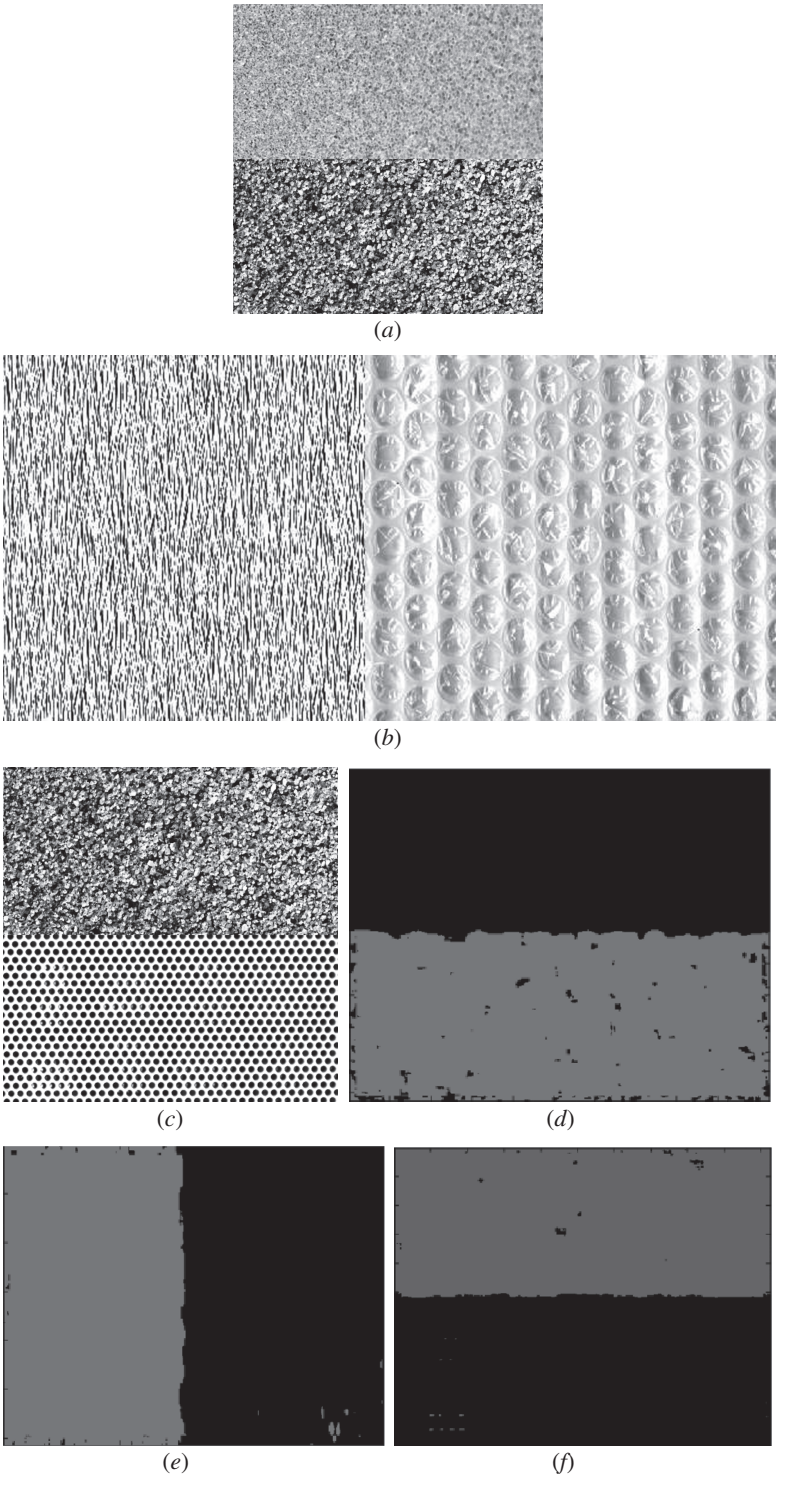

Figure 5. (*a*) Synthetic image 1, (*b*) synthetic image 2, (*c*) synthetic image 3, (*d*) result of textural segmentation for Image 1, (*e*) result of textural segmentation for Image 2 and (*f*) result of textural segmentation for Image 3.

Downloaded by [University of California, San Diego] at 22:47 28 September 2012

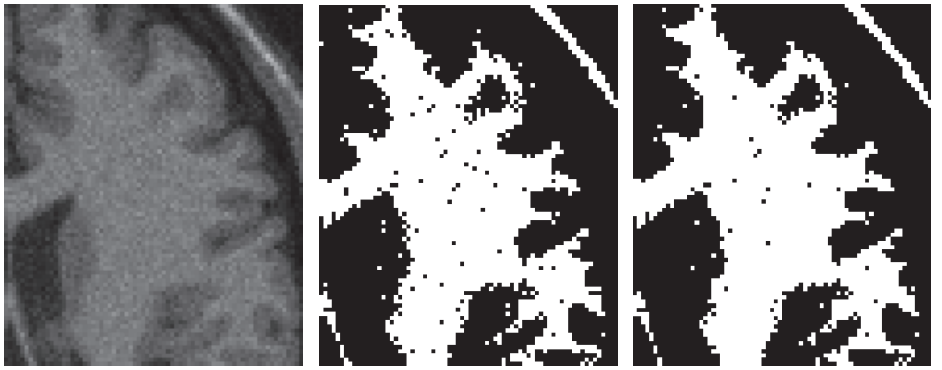

(*a*) (*b*) (*c*)

Figure 6. (*a*) Synthetic image, (*b*) result without NMAC and (*c*) smoothed result with NMAC.

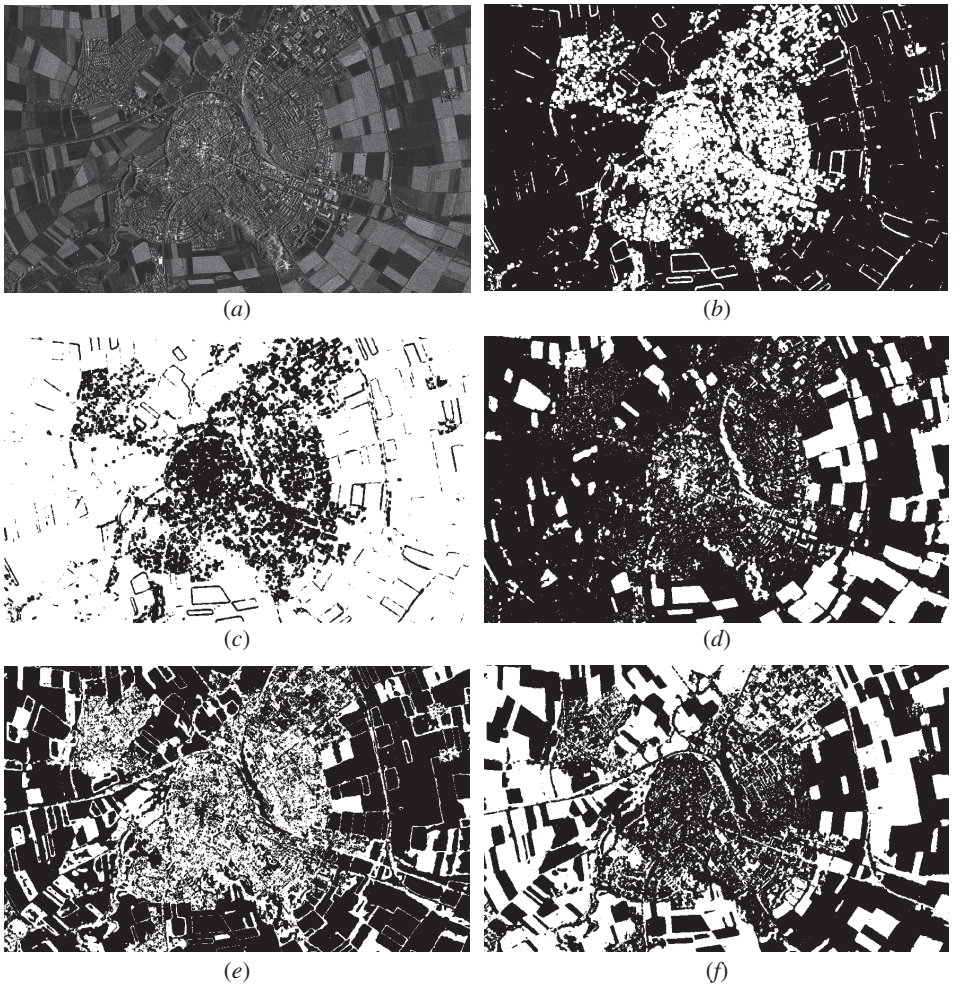

(*a*) (*b*) (*c*) (*d*) (*e*) (*f*)

Figure 7. (*a*) SAR image 1, (*b*) texture-based segmented region 1, (*c*) texture-based segmented region 2, (*d*) intensity-based segmented region 1, (*e*) intensity-based segmented region 2 and (*f*) intensity-based segmented region 3.

Downloaded by [University of California, San Diego] at 22:47 28 September 2012

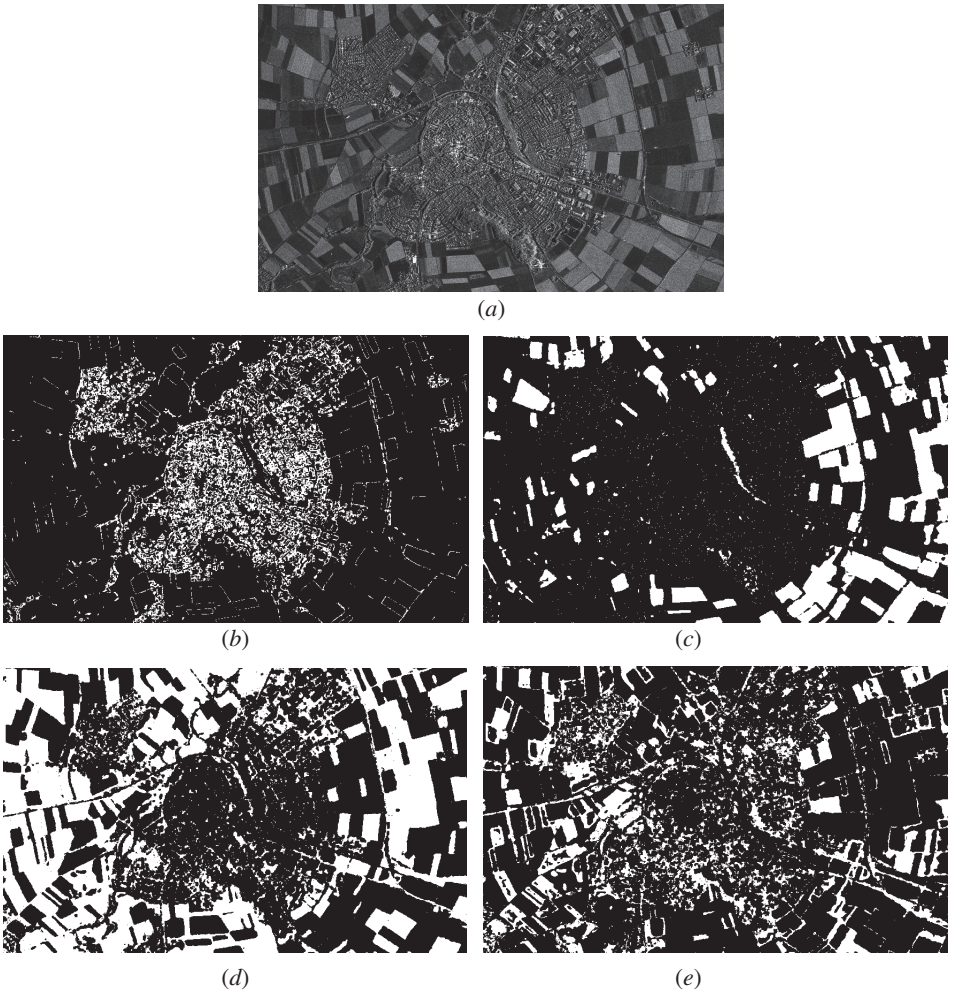

Figure 8. The results with the proposed algorithm: (*a*) SAR image 1, (*b*) inhabited area, (*c*) first farmland area, (*d*) second farmland area and (*e*) third farmland area.

using MFCM to yield texture-based classified results. For intensity-based segmentation, the original image is diffused using the SRAD technique followed by application of MFCM. This is followed by a unique method of end correction which levels the boundaries between two regions and also removes most of the pixel level noise. The results from the two parallel approaches are intersected to yield the final output.

Quantitative testing of the proposed technique of DSWSE and usage of undownsampled coefficient matrices has shown considerable enhancement in the accuracy of results. Also, the application of NMAC has been found to be quite efficient in improving the region boundaries and in removing the pixel level noise as predicted. Qualitative testing on actual SAR images clearly depicts the efficacy of this approach in real world applications. Thus, this algorithm is quite apt for practical purposes. The algorithm takes an average time of 5 minutes to segment a SAR image of dimensions 1130×1834 on Matlab^{TM} version 7.3 on a Pentium-4 2.1 GHz machine. The maximum

Downloaded by [University of California, San Diego] at 22:47 28 September 2012

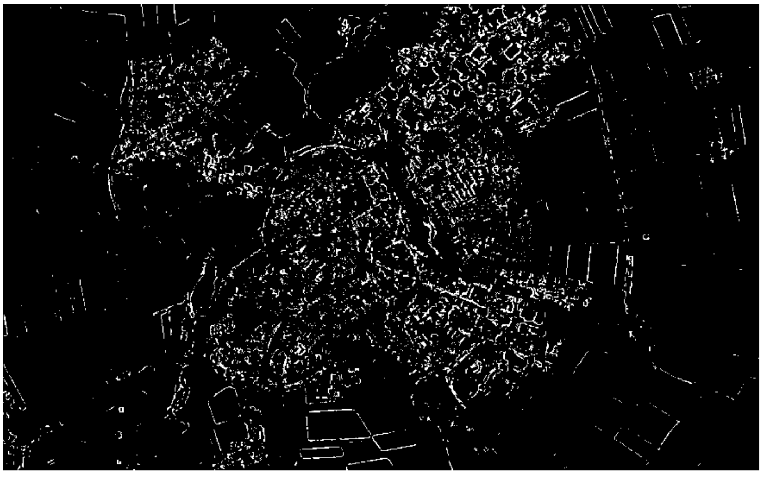

Figure 9. Output of the combination of non-corresponding interim results.

time is taken by the fuzzy algorithm that takes into account the spatial consideration. The overall time taken by the algorithm can be reduced by implementing the code on some low-level language like C/Python.

7. Limitations and future work

The main limitation of the proposed algorithm is that it is not fully automatic. The number of textural clusters needs to be perceived by the user and fed to the algorithm. Similarly the choice of the size of the sliding window for the DSWSE algorithm was found experimentally.

Future work on this algorithm will consist of steps to make it fully automatic, thereby limiting human intervention to a minimum level.

References

Ahmed, M.N., Yamany, S.M., Mohamed, N., Farag, A.A. and Moriarty, T., 2002, A modified fuzzy *c*-means algorithm for bias field estimation and segmentation of MRI data. *IEEE Transactions on Image Processing*, **21**, pp. 193–199.

Anbeek, M.P., Vincken, K.L., van Bochove, G.S., van Osch, M.J.P. and van der Grond, J., 2005, Probabilistic segmentation of brain tissue in MR imaging. *NeuroImage*, **27**, pp. 795–804.

Arivazhagan, S. and Ganesan, L., 2003, Texture segmentation using wavelet transform. *Elsevier Pattern Recognition Letters*, **24**, pp. 1531–1521.

Arivazhagan, S., Ganesan, L. and Priyal, S.P., 2006, Texture classification using Gabor wavelets based rotation invariant features. *Elsevier Pattern Recognition Letters*, **27**, pp. 1976–1982.

Bernad, G.P., Denise, L. and Refregier, P., 2007, Semi-automatic fast recognition of areas of interest for SAR image interpretation. In *IEEE Geoscience and Remote Sensing Symposium*, 23–28 July 2007, Barcelona, Spain, vol. 1, pp. 464–467 (New York: IEEE).

Buckreuss, S., Balzerm, W., Muhlbauer, P., Werninghaus, R. and Pitz, W., 2003, The terra SAR-X satellite project. *IEEE Geoscience and Remote Sensing Symposium*, **5**, pp. 3096–3098.

Downloaded by [University of California, San Diego] at 22:47 28 September 2012

CHANG, T. and KUO, C.-C. J., 1993, Texture analysis and classification with tree-structured wavelet transform. *IEEE Transactions on Image Processing*, **2**, pp. 429–441.

CHARALAMPIDIS, D. and KASPARIS, T., 2002, Wavelet-based rotational invariant roughness features for texture classification and segmentation. *IEEE Transactions on Image Processing*, **11**, pp. 825–837.

CHUMSAMRONG, W., THITIMAJSHIMA, P. and RANGSANSERI, Y., 2000, Synthetic Aperture Radar (SAR) image segmentation using a new modified fuzzy *c*-means algorithm. In *Proceedings of the International Geoscience and Remote Sensing Symposium*, July 2000, Honululu, HI, vol. 2, pp. 624–626 (New York: IEEE).

COHEN, F. S., FAN, Z. and PATEL, M.A., 1991, Classification of rotated and scaled textured images using Gaussian Markov random field models. *IEEE Transactions on Pattern Analysis and Machine Intelligence*, **13**, pp. 192–202.

DERIN, H. and ELLIOTT, H., 1987, Modeling and segmentation of noisy and textured images using Gibbs random fields. *IEEE Transactions on Pattern Analysis and Machine Intelligence*, **9**, pp. 39–55.

DUBUISSON-JOLLY, M.-P. and GUPTA, A., 2000, Color and texture fusion: application to aerial image segmentation and GIS updating. *Elsevier Image and Vision Computing*, **18**, pp. 823–833.

HALEY, G.M. and MANJUNATH, B.S., 1995, Rotation invariant texture classification using modified Gabor filters. In *International Conference on Image Processing*, Washington, DC, vol. 1, pp. 262–265 (New York: IEEE).

HARALICK, R.M., SHANMUGAM, K. and DINSTEIN, I.H., 1973, Textural features for image classification. *IEEE Transcations on Pattern Analysis and Machine Intelligence*, **3**, pp. 610–621.

LAINE, A. and FAN, J., 1993, Texture classification by wavelet packet signatures. *IEEE Transactions on Pattern Analysis and Machine Intelligence*, **15**, pp. 1186–1191.

LAM, S.W.-C., 1996, Texture feature extraction using gray level gradient based co-occurrence matrices. In *IEEE International Conference on Systems, Man, and Cybernetics*, July 1996, Beijing, China, vol. 1, pp. 267–271 (New York: IEEE).

LIN, J.-S., CHENG, K.-S. and MAO, C.-W., 1996, Segmentation of multispectral magnetic resonance image using penalized fuzzy competitive learning network. *Computers and Biomedical Research*, **29**, pp. 314–326.

MALLAT, S.G., 1989, A theory for multiresolution signal decomposition: the wavelet representation. *IEEE Transcations on Pattern Analysis and Machine Intelligence*, **11**, pp. 674–693.

MANJUNATH, B.S. and CHELLAPPA, R., 1991, Unsupervised texture segmentation using Markov random field models. *IEEE Transcations on Pattern Analysis and Machine Intelligence*, **13**, pp. 478–482.

PRATT, W.K., 2001, *Digital Image Processing*, 3rd edn., Chapter 10 (Los Altos, CA: John Wiley.

SAITO, T., KUDO, H. and SUZUKI, S., 1996, Texture image segmentation by optimal Gabor filters. In *Third International Conference on Signal Processing*, Beijing, China, vol. 1, pp. 380–383 (New York: IEEE).

SHARMA, R.K., KUMAR, B.S., DESAL, N.M. and GUJRATY, V.R., 2008, SAR for disaster management. *IEEE Aerospace and Electronics Systems Magazine*, **23**, pp. 4–9.

SUN, P., CHAIA, T. and ZHOU, X.-J., 2008, Rotary kiln flame image segmentation based on FCM and gabor wavelet based texture coarseness. In *Proceedings of the Seventh World Congress on Intelligent Control and Automation*, June 2008, Chongquing, China, pp. 7615–7620 (New York: IEEE).

UNSER, M., 1995, Texture classification and segmentation using wavelet frames. *IEEE Transactions on Image Processing*, **4**, pp. 1549–1560.

WU, J., POEHLMAN, S. and NOSEWORTHY, M.D., 2008, Texture feature based automated seeded region growing in abdominal MRI segmentation. In *International Conference*

Downloaded by [University of California, San Diego] at 22:47 28 September 2012

on BioMedical Engineering and Informatics, Sanya, Hainan, China, pp. 263–267 (New York: IEEE).

YONG, Y., CHONGXUN, Z. and PAN, L., 2004, A novel fuzzy *c*-means clustering algorithm for image thresholding. *Measurement Science Review*, **4**, pp. 13–19.

YU, Y. and ACTON, S.T., 2002, Speckle reducing anisotropic diffusion. *IEEE Transactions on Image Processing*, **11**, pp. 1260–1270.

ZIJDENBOS, A.P., DAWANT, B.M., MARGOLIN, R.A. and PALMER, A.C., 1994, Morphometric analysis of white matter lesions in MR images: method and validation. *IEEE Transactions on Medical Imaging*, **13**, pp. 716–724.

ZWIGGELAAR, R., 2004, Texture based segmentation: automatic selection of co-occurrence matrices. In *Proceedings of the 17th International Conference on Pattern Recognition*, Cambridge, UK, July 2004, vol. 1, pp. 588–591 (New York: IEEE).

Downloaded by [University of California, San Diego] at 22:47 28 September 2012

Downloaded by [University of California, San Diego] at 22:47 28 September 2012